16th World Conference on Earthquake, 16WCEE 2017

Santiago Chile, January 9th to 13th 2017

Paper N° 223

Registration Code: S-V1461566968

BASELINE EFFECT ON THE ESTIMATION OF CRUSTAL DISPLACEMENT USING GPS KINEMATIC RELATIVE POSITIONING

L. Moya[(1)], F. Yamazaki[(2)], W. Liu[(3)]

[(1)] *Graduate Student, Chiba University, Chiba, Japan, lmoyah@chiba-u.jp*
[(2)] *Professor, Chiba University, Chiba, Japan, fumio.yamazaki@faculty.chiba-u.jp*
[(3)] *Assistant Professor, Chiba University, Chiba, Japan, wen.liu@chiba-u.jp*

Abstract

The Global Navigation Satellite System (GNSS) has become an important technology with which to calculate the crustal deformation and displacement waves produced by earthquakes. In Japan, a dense GNSS network (GEONET) is available, with 1200 stations distributed uniformly throughout the country. Currently, relative positioning is one of the most precise GNSS positioning techniques, with a centimeter level of accuracy. However, this method requires two GNSS stations: a station where an estimation of displacement is to be determined and a station that remains stationary with a well-known position. To fulfill this requirement, the base station must be located far enough from the epicenter to assure that no displacement is produced. The performance of relative positioning depends on the distance between the receiver and the base stations, often referred to as the baseline. In this study, we evaluate this tradeoff by calculating the permanent displacement in the Geonet station 0266 during the November 22, 2014 Mw 6.2 Nagano earthquake several times with different base stations. Then, variations in the permanent displacement are evaluated in terms of the baseline. With several available GEONET stations to set as the base station, we study the relationship between the performance of displacement and the baseline.

Keywords: Crustal movement; GPS; GEONET; the 2014 Nagano earthquake, RTK positioning

1. Introduction

Crustal movement is important for early warning systems (EWSs) because it can be inverted to estimate the earthquake source parameters and to simulate the tsunami wave propagation [1, 2, 3]. Currently, three main technologies are used to estimate the permanent displacement due to crustal movement: accelerometers [4, 5, 6, 7], Synthetic Aperture Radar (SAR) data [8, 9, 10, 11], and the Global Navigation Satellite System (GNSS) [12, 13, 14]. Crustal deformation estimated from the double integration of acceleration records shows significant errors produced by the zero line shift [15]. The displacement from SAR has a low temporal resolution because it requires two images, constraining the measurement to the orbital period of the satellite. From GNSS, there are two methods to calculate displacement with high precision: Kinematic Precise Point Positioning (KPPP) and Real-Time Kinematic (RTK) positioning. KPPP has become more popular in recent years because it requires only one GNSS station; however, additional information, such as precise ephemerides and clock correction, which is provided by the International GNSS Service (IGS), is required. RTK requires two GNSS stations and achieves the best accuracy level under certain conditions. The present investigation attempts to evaluate the feasibility of using RTK to estimate coseismic displacements in cases where the |BL| ranges from 20 km to more than 1000 km. For this purpose, the November 22, 2014 inland earthquake in Nagano Prefecture, Japan is used as a case study because crustal deformation was observed in a narrow area.

2. Real-Time Kinematic Method

RTK aims to calculate, for each epoch, the vector between an unknown station (rover station) with respect to a station with well-known coordinates that must remain constant in time (master station). In other words, the relative position of the rover station with respect of the master station as a function of time. The vector between the two stations is known as the baseline (BL) vector. The method requires receivers that output the P code and carrier-phase observations on both frequencies L1 (1575.42 Hz) and L2 (1227.60 Hz). The P code is a sequence of approximately $2.35 \cdot 10^{14}$ chips (each chip represent a bit) with a chipping rate of 10.23 MHz, and is used to calculate the pseudorange. The carrier-phase is a measure of the carrier wave itself. The carrier phase and pseudorange equations for the master (point A) and the rover (point B) for a given satellite j with a frequency f are:

$$\begin{aligned}
\Phi_A^j(t) + f^j \delta^j(t) &= \frac{1}{\lambda}\rho_A^j(t) - \frac{1}{\lambda} I_A^j(t) + \frac{1}{\lambda} T_A^j(t) + N_A^j + f^j \delta_A(t) + \varepsilon_\Phi \\
\Phi_B^j(t) + f^j \delta^j(t) &= \frac{1}{\lambda}\rho_B^j(t) - \frac{1}{\lambda} I_B^j(t) + \frac{1}{\lambda} T_B^j(t) + N_B^j + f^j \delta_B(t) + \varepsilon_\Phi \\
P_A^j(t) + c\delta^j(t) &= \rho_A^j(t) + I_A^j(t) + T_A^j(t) + c\delta_A(t) + \varepsilon_P \\
P_B^j(t) + c\delta^j(t) &= \rho_B^j(t) + I_B^j(t) + T_B^j(t) + c\delta_B(t) + \varepsilon_P
\end{aligned} \tag{1}$$

where $\Phi_i^j(t)$ is the measured carrier phase expressed in cycles(see Figure 1), $P_i^j(t)$ is the pseudorange, λ is the wavelength, f^j is a signal frequency of the satellite j, c is the velocity of light, $\rho_i^j(t)$ is the geometric distance between the satellite j and the observed point i, $\delta^j(t)$ is the bias of the satellite clock j, $\delta_i(t)$ is the clock bias of the receiver at point i, $I_i^j(t)$ and $T_i^j(t)$ is the ionosphere and troposphere delay between the satellite j and the observed point i, and ε_Φ is the measurement error of carrier-phase. For shorth BL length (|BL|), the double differences of Eq. (1) are:

$$\begin{aligned}\Phi_{AB}^{jk}(t) &= \frac{1}{\lambda}\rho_{AB}^{jk}(t) + N_{AB}^{jk} + \varepsilon_{\Phi} \\ P_{AB}^{jk}(t) &= \rho_{AB}^{jk}(t) + \varepsilon_{P}\end{aligned} \tag{2}$$

which follows the symbolic convention:

$$\begin{aligned}*_{AB}^{j} &= *_{B}^{j} - *_{A}^{j} \\ *_{AB}^{jk} &= *_{AB}^{k} - *_{AB}^{j}\end{aligned} \tag{3}$$

When the |BL| is short, the ionosphere (I_i^j) and troposphere (T_i^j) delay are canceled in equation (2) because they are assumed to be equal for both the master and the rover station. A centimeter accuracy level is achieved when the |BL| is less than approximately 10-20 km [16, 17, 18]. Nevertheless, the permanent displacement required for EWS must be calculated under different conditions. A short |BL| is not useful because coseismic deformation is widely spread; therefore, permanent displacements would develop for both the master and rover stations when the |BL| is less than 20 km. Therefore, the RTK technique with a long |BL| is required. For a long |BL|, the atmospheric effects must be considered in the double-differencing equation (2).

$$\begin{aligned}\Phi_{AB}^{jk}(t) &= \frac{1}{\lambda}\rho_{AB}^{jk}(t) - \frac{1}{\lambda}I_{AB}^{jk}(t) + \frac{1}{\lambda}T_{AB}^{jk}(t) + N_{AB}^{jk} + \varepsilon_{\Phi} \\ P_{AB}^{jk}(t) &= \rho_{AB}^{jk}(t) + I_{AB}^{jk}(t) + T_{AB}^{jk}(t) + \varepsilon_{P}\end{aligned} \tag{4}$$

Because the assumption that ionosphere and troposphere delay are equal for both master and rover station is no longer acceptable, these terms must be estimated. Equations (2) and (4) represent the relation between two receivers and two satellite's signals. Furthermore, RTK method requires at least four satellites to set up a equations system necessary to calculate the coordinates of the receiver. Several models have been proposed for I_i^j and T_i^j, such as dual-frequency measurements to eliminate the ionosphere delay, and the Saastamoinen model for the tropospheric delay. Another strategy to solve equation (4) is to consider I_i^j and T_i^j as additional unknows by a non-linear combination [18].

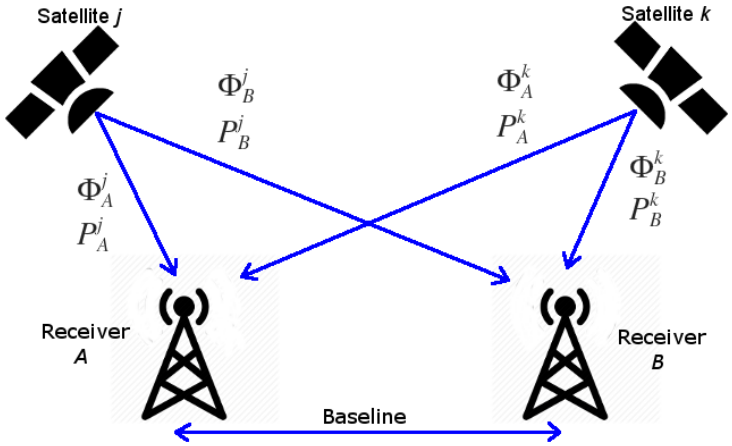

Figure 1. Principle of relative positioning

2. GEONET

The GNSS Earth Observation Network System (GEONET) of Japan began in 1996 with the join of the two GPS network systems: the Continuous Strain Monitoring System with GPS (COSMOS-G2) and the GPS Regional Array for Precise Surveying/Physical Earth Science (GRAPES) and an additional 400 station. Later on, in 2002 GEONET stations became usable for public surveys and in 2003 the Geospatial Information Authority of Japan (GSI), the institution in charge of GEONET, upgraded the GEONET system and added real-time capability.

Currently, GEONET consists of 1,300 stations located at intervals of approximately 20 km [13, 14] (Figure 1a). Only one antenna type, the choke ring antenna of Dorne Margolin T-type, is used in order to avoid multipath and different antenna phase center variations. Besides, the receivers are capable of 1-Hz sampling and real-time data transfer in a uniform format (RINEX - Receiver Independent Exchange Format). All the stations operate 24 hours a day and record the signal of the USA GPS, the Russian GLONASS and the Japanese QZSS. GEONET provides RINEX data with 30 second intervals through the internet and high-sampling rate data with 1 Hz sampling through a private distributor.

GEONET uses the data with 30-second sampling to perform three kinds of routine analysis: Quick, rapid and final analysis. Quick analysis is carried out every 3 hours using 6-hour data window and ultra-rapid products from the IGS, Rapid analysis is carried out every day with 24 hours of data and using ultra-rapid products as well. Final analysis is carried out every week but with two weeks of delay in order to use the IGS final products. An additional analysis is carried out in an emergency situation. Using 1 Hz real-time data, RTK analysis is performed.

The GEONET network is used to monitor long-term crustal movements, detect coseismic displacements, and detect volcanic activities. Besides, GEONET data has been used in other research areas such as geodesy, ionospheric research and so on.

3. Case Study

A Mw 6.7 earthquake occurred on November 22, 2014 in the northern part of Nagano Prefecture (Figure 2a), hereafter referred as the 2014 Nagano earthquake. The rupture process was at the NNE-WWS trending Kamashiro active fault [19]. A large coseismic displacement was detected at the GEONET Hakuba (with code 0266) control station. Figure 1b shows the displacement calculated from the daily coordinates published by GSI. Displacements of 12.3 cm in the vertical direction and 28.4 cm in the horizontal direction (24.4 cm to the east and 14.6 cm to the south) were detected, which agree with the quick estimation published by GSI (12 cm and 29 cm for the vertical and lateral components).

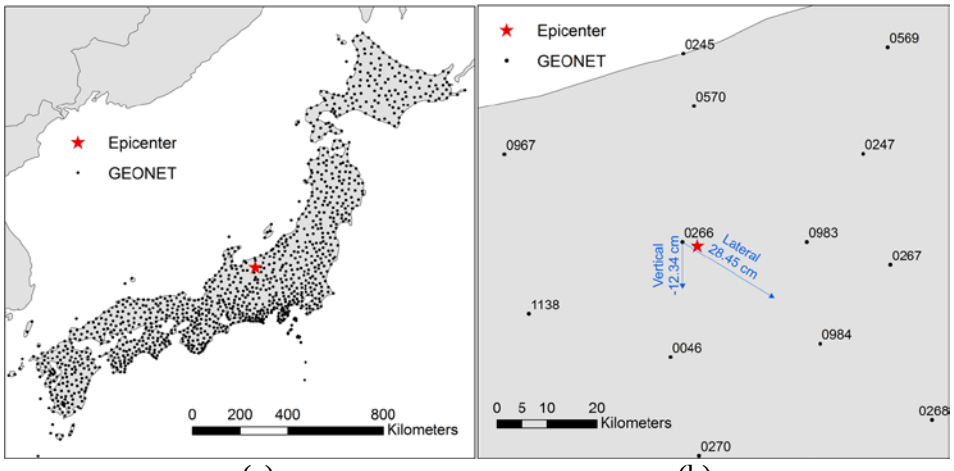

(a) (b)

Figure 2. (a) Distribution of GEONET stations and epicenter of the Nagano earthquake. (b) Location of the 0266 GEONET station and the coseismic displacement during the Nagano earthquake.

Table 1. Option settings for the two RTK methods

Option	Conventional	For long BL
Positioning mode	Kinematic	Kinematic
Frequencies	L1+L2	L1+L2
Receiver dynamics	OFF	OFF
Earth tides correction	OFF	ON
Elevation mask	10°	10°
Ionosphere correction	OFF	Estimate STEC
Troposphere correction	OFF	Estimate ZTD+Gradient
Satellite ephemeris	Broadcast	Precise
Ambiguity validation threshold	3.0	3.0
Min elevation to fix ambiguity	-	25
Min elevation to hold ambiguity	-	35
Code/Carrier-Phase error ratio	100	100
Carrier phase error	0.003+0.003/sin El m	0.003+0.003/sin El m
Process noise of vertical iono. delay	10^{-3} m/sqrt(s)	10^{-3} m/sqrt(s)
Process noise of ZTD	10^{-4} m/sqrt(s)	10^{-4} m/sqrt(s)
Satellite antenna model	IGS08.ATX	IGS08.ATX
Receiver antenna model	IGS08.ATX	IGS08.ATX

Only the GEONET Hakuba (0266) station recorded a large displacement; the second largest displacement was recorded at station 0984 (see Figure 2b), with a lateral displacement of only 1.7 cm. The permanent displacement developed locally in the Nagano earthquake makes it suitable to evaluate the effect of the |BL| in the performance of the RTK method using different pairs of GEONET control stations. For each pair, the rover station is fixed as the 0266 control station and the master station changes continuously, assuming no permanent displacement. A total of 1,220 pairs of GEONET control stations with the |BL| ranging from 20 km to approximately 2,000 km was used for the evaluation.

4. Method

Two configuration settings were chosen in this study. One is the conventional RTK (CRTK) method used for a short |BL| (less than approximately 20 km), where a centimeter level of accuracy is guaranteed. Because this setting is designed for a short |BL|, atmospheric correction is not applied. The second configuration setting is the one currently used in the Japanese Tsunami EWS [1], where the atmospheric correction and precise ephemerides are necessary. This second configuration is designed for long-|BL| RTK (LRTK). A complete description of the method can be found in Takasu and Yasuda's paper [18]. The details of the configuration of each option are depicted in Table 1. In this study, the open source program package for GNSS positioning, RTKLIB (www.rtklib.com; last accessed on January 10, 2016), was used to process the data.

The RINEX data for 30 second intervals from each control station provided by the GSI server (ftp://terras.gsi.go.jp/; last accessed on January 19, 2016) were used in this research. The precise coordinates for the master stations were obtained from the daily coordinate product of November 21, 2014, which is one day before the Nagano earthquake. Because the method is intended to work in real-time for EWS, the ultra-rapid product of the ephemerides, which is provided in near real-time by the IGS (https://igscb.jpl.nasa.gov/components/prods.html; last accessed on January 19, 2016), is used.

5. Results

Figure 3 shows the displacement time history obtained from RTK for the two configuration settings mentioned above. Fifteen minutes of record are depicted to show five minutes before and 10 minutes after the origin time of the earthquake, which was at UTC 13:08 according to the National Research Institute for Earth Science and Disaster Prevention (NIED) of Japan. As a reference to evaluate the results, the displacement obtained from the daily coordinate products is also depicted in Figure 3 (red line). The results have been separated according to the |BL| magnitude into four groups: |BL| less than 50 km (12 control stations), |BL| between 50 km and 100 km (49 control stations), |BL| between 100 km and 500 km (676 control stations), and |BL| greater than 500 km (483 control stations). For each record, an average of the first 5 minutes of record was removed.

As expected, for the results using CRTK (Figure 3a), errors increase with increasing |BL|. Some records of the first group show a *cycle slip effect*, which means a reinitialization of the counter of the integer number of cycles of the signal that is caused by the signal lock. For a |BL| less than 100 km, the displacement is easily depicted. However, the results from the 3rd and 4th groups show high distortions. However, in most of the records, these distortions show either increasing or decreasing trends in time, and with some effort, the coseismic displacement could be observed. These trends represent the systematic errors produced by the atmospheric effects. A problem arises of how to identify a coseismic displacement based on the displacement from the trend produced by the atmospheric effects. However, the shape of the coseismic displacement is a sudden action similar to a step or ramp function, whereas the effect of the atmosphere is a continuous smooth change of the coordinate in time. Moreover, if accelerometers are available, which is highly probable because accelerometers are ubiquitous in seismic prone areas in Japan, the time when the coseismic displacement started is known.

Figure 3b shows the displacement time histories using the LRTK method for long |BL| lengths. Most of the systematic errors produced by the atmospheric effects have been significantly reduced. The cycle slip effect observed in the first group was almost eliminated. However, in the 2nd, 3rd and 4th groups, there are still some records that show high distortions. These records that show distortions without any trend depend on factors different from the atmospheric effects, such as a loss of signal. For instance, Figure 4 shows a case in which GEONET control station 1133 is selected as the master. There was a loss of signal of the GPS24 satellite when the initial part of the earthquake was coming. A closer look revealed that when the elevation angle of the GPS24 satellite reached 20º, the signal was blocked by a bamboo forest. Figures 4a and 4c show a contrast of the results with and without the signal of GPS24 using the CRTK method. Because the GPS24 has been removed, the coseismic displacement and the systematic error caused by the atmosphere could be observed. The loss of signal did not significantly affect the result when the LRTK method was applied (Figure 4b); however, an improvement was observed when the GPS24 signal was not considered in the process (Figure 4d).

Our main purpose is to evaluate the coseismic displacement rather than the accuracy of the coordinates calculated by the RTK. Thus, the displacement was estimated as the difference between the average of the first three records after coseismic displacement and the average of the three records before coseismic displacement. Figure 5 shows the coseismic displacements calculated from RTK for different the |BL| lengths, shown as black dots. In the figure, the horizontal blue dashed line represents the coseismic displacement estimated from the daily coordinates. There is a clear decrease of the accuracy in the estimation of the displacement when the BL length increases in the results of CRTK (Figure 5a). The displacement could be estimated with a gradual increase of error until approximately 800 km, and after that, a significant increase of errors is observed. However, there is a slightly increase of error when LRTK is used, even for BL greater than 1,000 km.

For a closer look at the error, the difference between the coseismic displacement from the daily coordinates and from RTK is shown in Figure 6 as green dots. For a clear visualization on the error trend, a window averaging 50 km lengths is shown as red lines. Figure 6 also shows the average window plus two times its standard deviation (blue lines). The peaks observed in the red and blue lines are due to spurious results, such as the case shown in Figure 4. If the peaks observed in the blue lines are neglected, most of the errors are less than 10 cm for LRTK. For CRTK, as expected, the error increases with the increase in |BL|. For a |BL| less than 500 km, the errors are less than 20 cm but increase to 1 m when the |BL| is approximately 1,500 km.

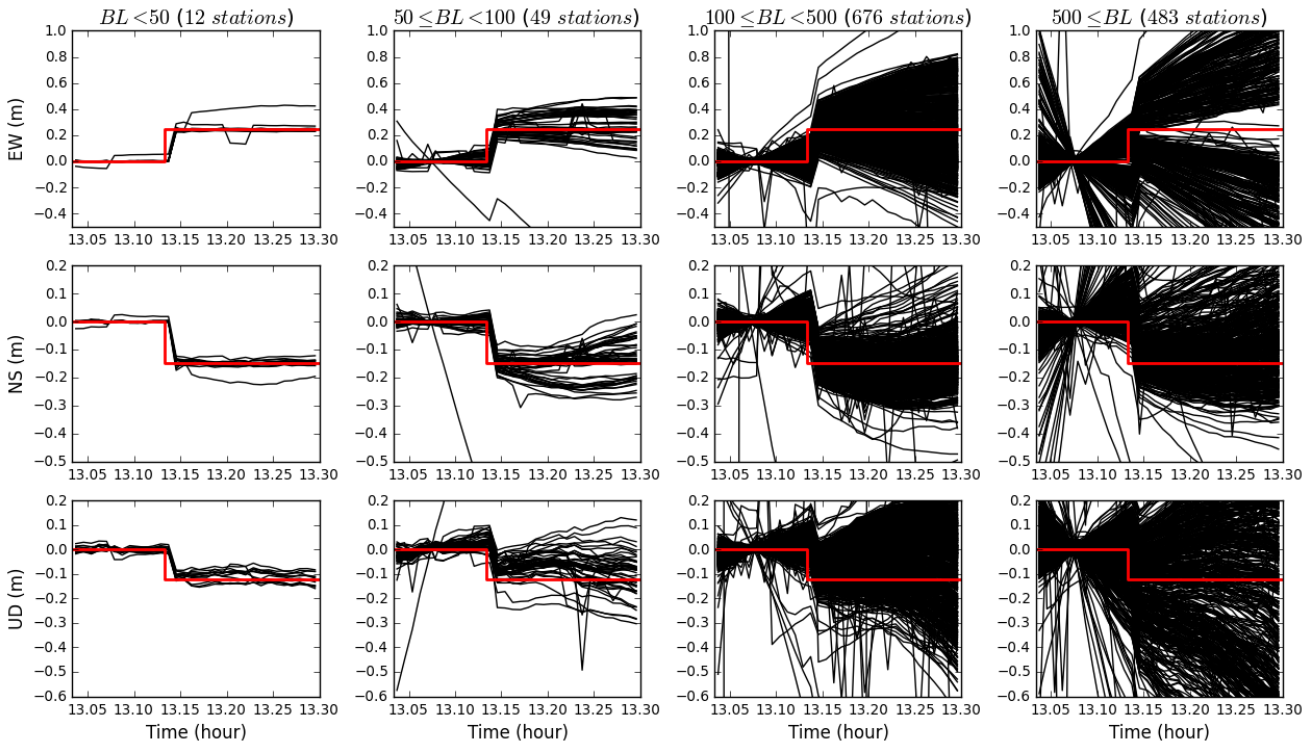

(a)

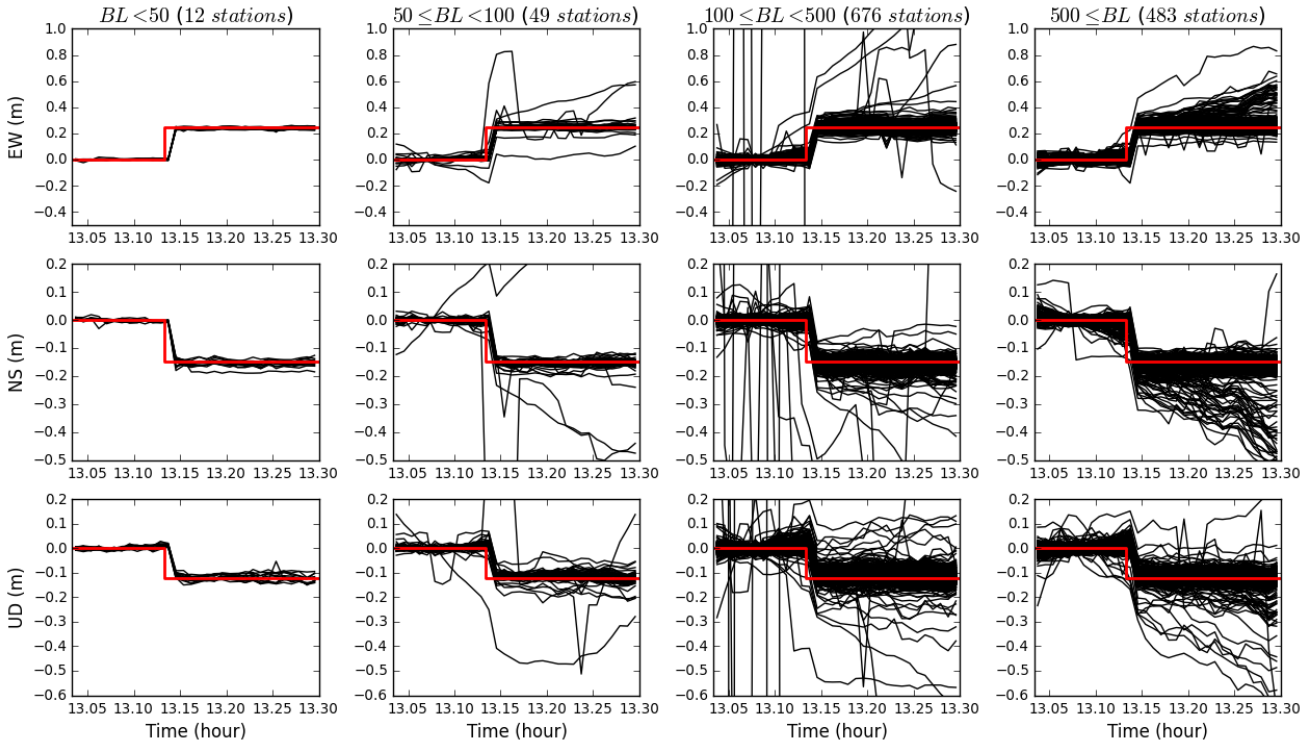

(b)

Figure 3. Displacement time histories obtained by (a) CRTK and (b) LRTK.

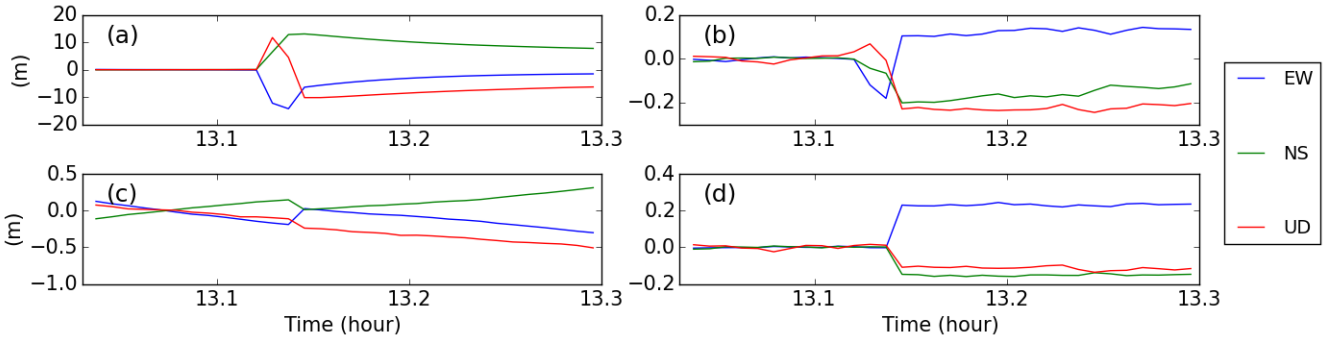

Figure 4. Displacement time histories at control station 0266 from the RTK method using station 1133 as the master station. (a) CRTK considering the GPS24 signal; (b) LRTK considering the GPS24 signal; (c) CRTK without the GPS24 signal; (d) LRTK without the GPS24 signal.

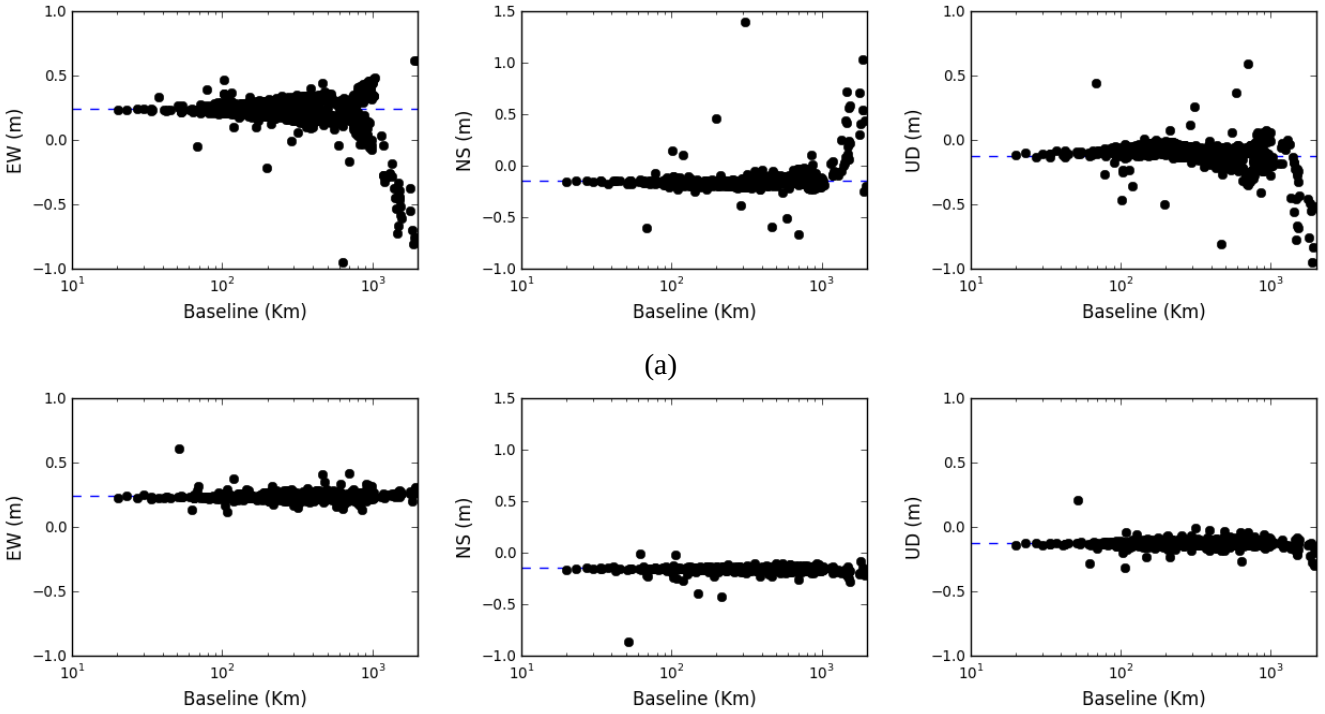

Figure 5. Calculated relative displacements with respect to the |BL| obtained by (a) CRTK and (b) LRTK.

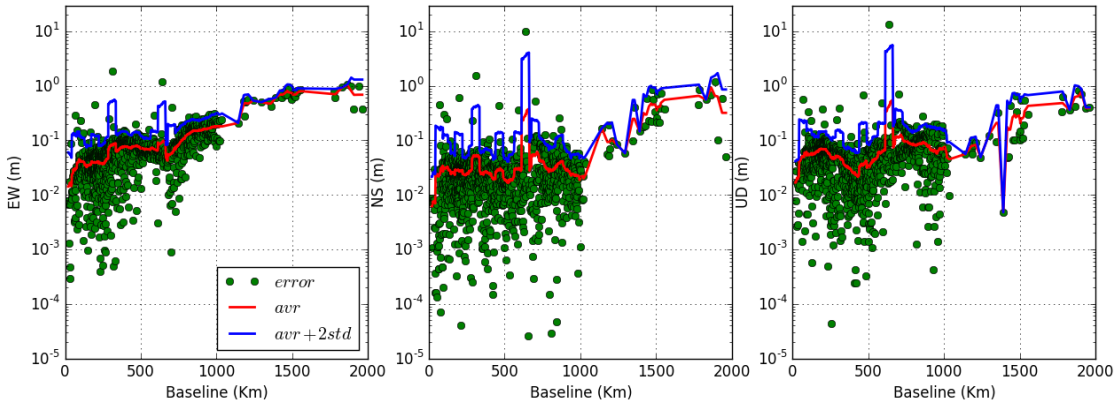

(a)

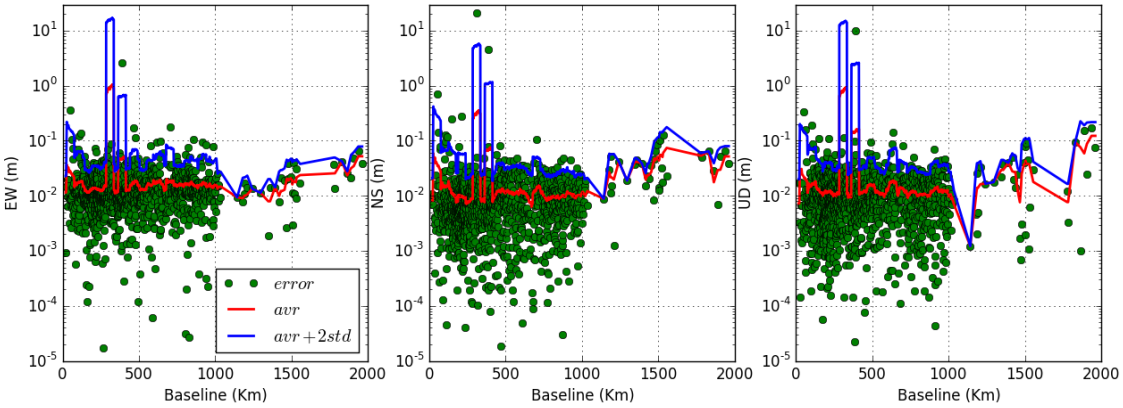

(b)

Figure 6. Difference between the coseismic displacement calculated from the RTK and from the daily coordinates for (a) CRTK and (b) LRTK.

6. Conclusions

In this paper, we studied the performance of Real-Time Kinematic (RTK) positioning for different baseline distances to assess coseismic deformation. For this purpose, the coseismic displacement recorded at one GNSS station during the November 22, 2014 Nagano earthquake was used. A total of 1,220 cases with BL lengths ranging from 20 km to approximately 2,000 km were evaluated. For each case, two setting processes were applied: the conventional RTK (CRTK), which is designed to achieve centimeter-level accuracy for BL lengths less than 20 km, and an RTK method designed for long baselines (LRTK).

Systematic errors appeared in the displacement time history for CRTK, resulting in a continuous and smooth change in the coordinates. The rate of those changes increases as the baseline increases. However, because the coseismic displacement occurs suddenly, it could be still observed in most cases. The systematic errors were almost removed when LRTK was used. Moreover, records with large distortions were still observed. These errors were attributed to factors other than the atmospheric effects.

For the studied case, the Nagano earthquake, the coseismic displacement estimated by the LRTK has errors less than 10 cm. However, the results from the CTRK have increasing errors as the baseline increases. These errors are less than approximately 20 cm for baselines less than 500 km and increase to one meter when the baseline reaches approximately 1,500 km. For the records with the shortest baseline, by comparing the blue lines of Figure 6 (the averaging window plus two times the standard deviation), CRTK achieves better results than LRTK. One reason for the better results is that the window averaging is affected by the large error caused by factors other than the baseline length; another reason is that for short baselines, using only double differentiation, more accurate atmospheric effects can be obtained than by estimating the atmospheric effects.

The atmospheric effects can then be removed because the atmospheric conditions in both control stations (rover and master) are well-correlated when the baseline is short.

7. References

[1] Ohta Y, Kobayashi T, Tsushima H, Miura S, Hino R, Takasu T, Fujimoto H, Iinuma T, Tachibana K, Demachi T, Sato T, Ohzono M, Umino N (2012): Quasi real-time fault model estimation for near-field tsunami forecasting based on RTK-GPS analysis: Application to the 2011 Tohoku-Oki earthquake (Mw 9.0). *Journal of Geophysical Research* **117**, B02311, 16p.

[2] Melgar D, Bock Y (2013): Near-field models with rapid earthquake source inversions from land- and ocean-based observations: The potential for forecast and warning. *Journal of Geophysical Research: Solid Earth* **118**, 1-17.

[3] Melgar D, Bock Y (2015): Kinematic earthquake source inversion and tsunami runup prediction with regional geophysical data. Journal of Geophysical Research: Solid Earth **120**, 1-26.

[4] Wu Y, Wu C (2007): Approximate recovery of coseismic deformation from Taiwan strong-motion records. *Journal of Seismology* **11**, 159-170.

[5] Chao W, Wu Y, Zhao L (2010): An automatic scheme for baseline correction of strong-motion records in coseismic deformation determination. *Journal of Seismology* **14**, 495-504.

[6] Wang R, Schurr B, Milkereit C, Shao Z, Jin (2011): An improved automatic scheme for empirical baseline correction of digital strong-motion records. *Bulleting of the Seismological Society of America* **101**, 2029-2044.

[7] Moya L, Yamazaki F, Liu W (2015): Comparison of coseismic displacement obtained from GEONET and seismic networks. Journal of Earthquake and Tsunami. (In process – accepted in 2016).

[8] Liu W, Yamazaki F, Matsuoka T, Nonaka T, Sasagawa T (2015): Estimation of three-dimensional crustal movements in the 2011 Tohoku-Oki, Japan, earthquake from TerraSAR-X intensity images. *Natural Hazards and Earth System Sciences* **15**,637-645.

[9] Liu W, Moya L, Yamazaki F (2015): Extraction of coseismic displacement in the November 22, 2014 Nagano, Japan earthquake from ALOS-2 images. *The 5th Asia-Pacific conference on synthetic aperture radar*, 845-848.

[10] Liu W, Yamazaki F (2013): Detection of crustal movement from TerraSAR-X intensity images for the 2011 Tohoku,Japan earthquake. *IEEE Geoscience and Remote Sensing Letters* **10** (1), 199-203.

[11] Imakiire T, Kobayashi T (2011): The crustal deformation and fault model of the 2011 off the Pacific Coast of Tohoku earthquake. Bulleting of the Geospatial Information Authority of Japan **59**,21-33.

[12] Ozawa S, Nishimura T, Suito H,Kobayashi T, Tobita M, Imakiire T (2011): Coseismic and postseismic slip of the 2011 magnitude-9 Tohoku-Oki earthquake. *Nature* **475** (7356), 373-377.

[13] Sagiya T (2004): A decade of GEONET: 1994-2003 The continuous GPS observation in Japan and its impact on earthquake studies. *Earth Planets Space* **56**, xxix-xli.

[14] Yamagiwa A, Hatanaka Y, Yutsudo T, Miyahara B (2006): Real-time capability of GEONET system and its application to crust monitoring. *Bulleting of the Geographical Survey Institute* **53**, 27-33.

[15] Boore D (2001): Effect of baseline corrections on displacement and response spectra for several recordings of the 1999 Chi-Chi, Taiwan, Earthquake. *Bulleting of the Seismological Society of America* **91**, 1199-1211.

[16] Hofmann-Wellenhof B, Lichtenegger H, Collins J (2001): GPS Theory and practice. Springer-Verlag Wien, USA, 5th edition.

[17] Borre K, Stran G (2012): *Algorithms for global positioning*, Wellesley-Cambridge, USA.

[18] Takasu T, Yasuda A (2010): Kalman-filter-based integer ambiguity resolution strategy for long-baseline RTK with ionospheric and tropospheric estimation. *23rd International Technical Meeting of the Satellite Division*, Inst. of Nav., Oreg., 21-24 Sept.

[19] Hata Y, Murata A, Miyajima M (2015): Preliminary report on strong motion estimation at damage and non-damaged clusters in Kamashiro district, Hakuba Village during large earthquake (M_{JMA}=6.7) in northern Nagano Prefecture, centra Japan. *JSCE journal of Disaster FactSheets* **FS2015-E-0001**, 9 pages.